Acta Pharmaceutica Sinica B 2026;16(7):4676−4691

Chinese Pharmaceutical Association
Institute of Materia Medica, Chinese Academy of Medical Sciences

Acta Pharmaceutica Sinica B

www.elsevier.com/locate/apsb
www.sciencedirect.com

ORIGINAL ARTICLE

In situ generation of EBNA1 CAR-T cells eradicates antigen specific auto-immune B cells for multiple sclerosis treatment

Chongdeng Shi[a,b,†], Maosen Han[b,†], Hui Yang[c,†], Xiaotian Zhao[b], Zuolin Zheng[b], Huijun Wang[c], Zhipeng Fu[b], Kuan Dai[e], Kun Zhao[b], Na Li[d], Yudong Song[b,*], Chen Chen[b,*], Fei Yang[b,*], Anning Li[c,*], Xinyi Jiang[b,*]

[a]*Clinical Innovation & Research Center (CIRC), Shenzhen Hospital, Southern Medical University, Shenzhen 518100, China*
[b]*State Key Laboratory of Discovery and Utilization of Functional Components in Traditional Chinese Medicine, NMPA Center for Innovation and Research in Regulatory Science, Shandong Key Laboratory of Targeted Drug Delivery and Advanced Pharmaceutics, Shandong Basic Science Special Academic Zone(Pharmacy) and Key Laboratory of Chemical Biology (Ministry of Education), Department of Pharmaceutics, School of Pharmaceutical Sciences, Cheeloo College of Medicine, Shandong University, Jinan 250012, China*
[c]*Department of Radiology, Qilu Hospital, Shandong University, Jinan 250012, China*
[d]*College of Chemistry, Chemical Engineering and Materials Science, Shandong University, Jinan 250012, China*
[e]*Nanjing Foreigin Language School Xianlin Campus, Nanjing 210000, China*

Received 27 August 2025; received in revised form 23 October 2025; accepted 9 December 2025

KEY WORDS

Immunoengineering;
CNS;
Autoimmune disease;
B cell;
CAR-T;

Abstract Multiple sclerosis (MS) is a chronic inflammatory demyelinating disease of the central nervous system (CNS). Epstein−Barr virus (EBV)-induced B-cell overactivation could lead to inflammatory injury to the CNS, which is thought to underlie the initiation and progression of MS. To specifically eradicate these B cells, we report *in situ* EBNA1-specific chimeric antigen receptor (CAR)-T cells that were transiently programmed with circular RNA (circRNA)-laden CD7-targeted lipid nanoparticles (CD7-LNP). We demonstrate that systematic injection of CD7-LNP can efficiently introduce CAR circRNA

*Corresponding authors.
E-mail addresses: xinyijiang@sdu.edu.cn (Xinyi Jiang), anningli00@163.com (Anning Li), yangfei@sdu.edu.cn (Fei Yang), 201820601@mail.sdu.edu.cn (Chen Chen), 15110700038@fudan.edu.cn (Yudong Song).
[†]These authors made equal contributions to this work.
Peer review under the responsibility of Chinese Pharmaceutical Association and Institute of Materia Medica, Chinese Academy of Medical Sciences.

https://doi.org/10.1016/j.apsb.2026.03.033

Lipid nanoparticles;
Multiple sclerosis;
EAE

to T lymphocytes and yield *in vivo* CAR-T cells. These *in situ* CAR-T cells were able to specifically clear EBNA1-specific B cells and significantly mitigate the progression of MS in a MS mouse model. Thus, *in situ* generation of EBNA1-specific CAR-T cells hold promise as a therapeutic strategy for MS that avoids the risks of general immunosuppression, and warrant further clinical trials.

1. Introduction

Multiple sclerosis (MS) is an autoimmune neurological disorder of the central nervous system (CNS) of unknown aetiology[1,2]. The elevated Epstein−Barr virus (EBV) specific antibody titers and symptomatic primary EBV infections being epidemiologically associated with MS. EBV is a B cell-tropic virus, and B cells appear central to driving autoreactive pathogenic T cells in MS. EBV can trigger MS through molecular mimicry, promoting memory B cells that act as pro-inflammatory antigen-presenting cells for T cells, and by establishing a latent infection within B cells[3-6]. As such, tracking and eradicating these B cells may be a potential approach for MS therapy, which remains largely unexplored.

Large-scale clinical trials have demonstrated the efficacy of B-cell depletion therapy using the anti-CD20 monoclonal antibody (mAb) ocrelizumab in relapsing as well as primary progressive MS[7,8]. However, B-cell depletion therapy is often accompanied by the occurrence of infection risks[9,10]. EBV nuclear antigen 1 (EBNA1)-specific B cells that express an anti-EBNA1 BCR, a membrane-bound autoantibody, preferentially migrate to the CNS, contributing to CNS pathogenic autoimmunity in MS[11]. To direct EBNA1-specific rather than total B-cell depletion, we proposed engineering T cells with an EBNA1 chimeric autoantibody receptor (EBNA1-CAR) to achieve precise eradication of B cells, avoiding the potential risks associated with total B-cell depletion.

The current manufacturing process of CAR-T cells is labor-intensive and time-consuming and requires dedicated equipment and considerable technical expertise, limiting broader applications[12-−14]. As an alternative, *in vivo* programming of T cells to express CAR has emerged as a promising strategy. This approach leverages off-the-shelf products, offering key advantages such as reduced production costs and potentially enhanced therapeutic performance and safety[15]. mRNA-based CAR-T cell therapies have been successfully tested in preclinical and clinical settings across multiple cancers, including acute lymphoblastic leukemia (ALL), melanoma, and Hodgkin's lymphoma[16]. To simplify the complex manufacturing process of *ex vivo* CAR-T cells, we sought to engineer CAR-T cells *in vivo* by using targeted lipid nanoparticles (LNPs). CD7 is a single-domain Ig superfamily molecule expressed on T and NK cells, as well as on cells in the early stages of T cell differentiation and it will be rapidly internalized after binding to antibodies or antibody derivatives[17-19]. Thus, circRNA enveloped with EBNA1 chimeric autoantibody receptor (EBNA1-CAR) was packaged with the targeted LNP that was decorated with CD7 antibodies (Abs) for T-cell-targeted gene delivery. We firstly induced experimental allergic encephalomyelitis (EAE) with EBNA1 peptide (Supporting Information Fig. S1) and found intravenous injection of B cells from EAE mice aggravated EAE (Supporting Information Fig. S2). And, depletion B cell with CD19 Ab mitigated EAE severity (Supporting Information Fig. S3). Further, EBNA1-specific T cells were transferred alone or co-transferred with EBNA1 specific B cell into WT mice. And in the presence of EBNA1 specific B cells, disease onset occurred earlier, and the incidence and severity of clinical deficits were increased (Supporting Information Fig. S4). And we found that CD7-tagged LNPs (CD7/LNP) were able to efficiently deliver targeted circRNA to T lymphocytes and generate functional CAR-T cells *in situ*, which could specifically clear EBNA1-specific B cells and attenuate the progression of MS without the risk of potential infection, as demonstrated in an EAE mouse model (Fig. 1A).

2. Materials and methods

2.1. Cell line

CTLL-2 cells were obtained from the Institute of Biochemistry and Cell Biology, Shanghai Institutes for Biological Sciences, Chinese Academy of Sciences (Shanghai, China). The cells were cultured in RPMI 1640 medium supplemented with 10% (*v*/*v*) FBS, 100 U/mL penicillin, 100 U/mL streptomycin and 50 ng/mL IL-2 at 37 °C in a humidified atmosphere of 5% CO_2.

2.2. Animals models

SJL/J mice (female, aged 8 weeks) were obtained from Vitalriver Biotech. All animal experiments were conducted in accordance with the guidelines and regulations of Institutional Animal Care and Use Committee of the Cheeloo College of Medicine, Shandong University (approval number: 21074). The mice were housed under controlled conditions with a target temperature range of 19−25 °C and relative humidity of 30% to 60%. A time-controlled lighting system was used to provide a 12 h light/12 h dark cycle. Multiple sclerosis is female preponderance in prevalence. Female mice were used to allow for group housing throughout the study.

For active EAE, mice were immunized subcutaneously with $EBNA1_{AA411-426}$ (350 μg per mouse, peptide sequence: EADYFEYHQEGGPDGE) mixed with CFA emulsion (200 μL per mouse, Sigma−Aldrich, F588). Additionally, SJL/J mice were intravenously injected with pertussis toxin (350 ng per mouse, LIST Biological laboratories, Inc., 180222A1) at the time of immunization and 48 h later. For treatment, CD7/EBNA1/LNP (0.5 mg of circRNA/kg) and CD19 Ab (125 μg per mouse, three times every 7 days) were infused i.v. in EAE model mice on Day 9 when the disease phenotype was obvious (average score $\geq$1). Mice were scored for clinical symptoms and signs of EAE were translated into the clinical score as follows[20,21]: 0, no detectable signs of EAE; 0.5, tail weakness; 1, complete tail paralysis; 2, partial hindlimb paralysis or ataxia; 2.5, unilateral complete hindlimb paralysis; 3, complete bilateral hindlimb paralysis or severe ataxia; 3.5, complete hindlimb paralysis and partial forelimb

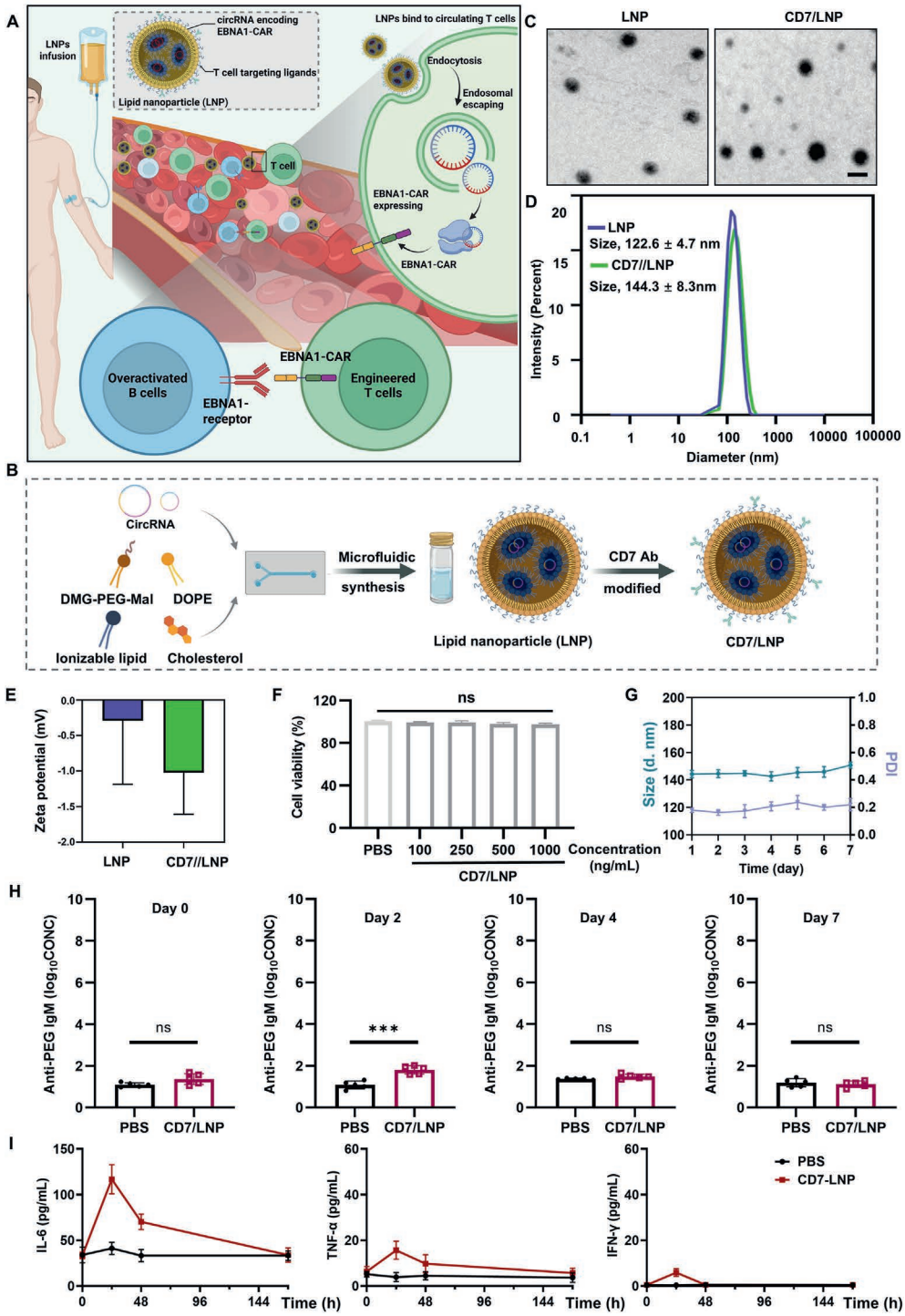

Figure 1 Construction and characterization of CD7/LNP. (A) Schematic illustration of CD7/LNP for *in situ* generation of EBNA1-CAR-T cells for MS therapy in EAE mouse model. (B) Synthesis of LNP and CD7/LNP with microfluidics. (C−E) Characterization of CD7/LNP. Scale bars = 200 nm. TEM images of non-targeted LNPs and (left panel) and CD7 targeted LNPs (right panel) after 12 h incubation in PBS (C). Hydrodynamic size distribution (D) and ζ potential of LNP and CD7/LNP (E). (n = 3 biological replicates). (F) Mouse primary T cells were co-cultured with CD7/LNP for 24 h and the effect of CD7/LNP on cell viability was evaluated using CCK-8. (n = 5, biological replicates). Data are presented as mean ± SD; ns, not significant. (G) Stability of CD7/LNP in PBS, as evaluated by determining changes in the nanocomplex size by DLS over 7 days. (n = 3 biological replicates). (H, I) CD7/LNP was administered to WT mice, blood samples were collected at Days 0, 2, 4 and 7, anti-PEG IgM levels (H) and immunogenicity assessment related cytokine (IL-6, TNF-α, and IFN-γ) (I) were measured with ELISA (n = 5 mice per group, biological replicates). Data are presented as mean ± SD, ***$P < 0.001$ *vs*. indicated; ns, not significant.

paralysis; 4, total paralysis of forelimbs and hindlimbs (mice with a score >4 were killed); and 5, death.

2.3. General synthetic procedures and spectral data

To a mixture of TBSCI (6.715 g, 44.6 mmol), imidazole (6.304 g, 92.9 mmol), TRIS (1.54 g, 12.4 mmol) was added 5 mL anhydrous DMF, reacted for 12 h at room temperature. CH_2Cl_2 was added to extract, and washed with saturated $NaHCO_3$ and saturated NaCl solution. The organic layer was collected and dried by anhydrous $MgSO_4$, filtered, and concentrated by rotary evaporation. The products were separated and purified by column chromatography to obtain Compound **1**.

To a mixture of 4-methyl-1-piperazineacetic acid (1.5 g, 6.32 mmol) with CH_2Cl_2 (10 mL) under stirring at 0 °C, 7.2 mL of TEA was added dropwise and reacted for 10 min; Subsequently, EDCI (1.8 g, 9.39 mmol) and HOBt (1.26 g, 9.32 mmol) were added and reacted for 30 min; Compound **1** (3.0 g, 6.47 mmol) dissolved in an appropriate amount of CH_2Cl_2 was dropped into the above system and reacted for 24 h. The reactants were washed and the organic layer was collected, dried with anhydrous MgSO4, filtered and concentrated. The products were separated and purified by column chromatography to obtain Compound **2**.

865 mg (2.73 mmol) TBAF·$3H_2O$ was dissolved in THF, dropped into a mixture of 500 mg (0.828 mmol) Compound **2** with 10 mL THF at 0 °C. The solvent was removed by rotary evaporation after reaction for 3 h, resulting in a pale oil (Compound **3**). The product can participate in the next reaction without purification. Compound **3** was dissolved in CH_2Cl_2, DCC (563 mg, 2.73 mmol) and DMAP (334 mg, 2.73 mmol) were added, and linoleic acid (765 mg, 2.73 mmol) was added at 0 °C. The reaction was stirred for 24 h; The reactants were washed and the organic layer was collected, dried with anhydrous $MgSO_4$, filtered and concentrated. The products were separated and purified by column chromatography to obtain Compound **4**.

2.4. LNP anti-CD7 antibody conjugation

To prepare antibody-targeted LNPs, LNPs were conjugated with purified mouse anti-CD7, as described previously[22]. Briefly, LNP was modified with maleimide functioning groups (DSPE-PEG-Mal). The antibody was functionalized with SATA (*N*-succinimidyl *S*-acetylthioacetate) to introduce sulfhydryl groups allowing conjugation to maleimide. SATA was deprotected using 0.5 mol/L hydroxylamine followed by removal of the unreacted components by G-25 Sephadex Quick Spin Protein columns. The reactive sulfhydryl group on the antibody was then conjugated to maleimide moieties using thioether conjugation chemistry. LNPs were combined with CD7 antibody at a molar ratio of 1:1 maleimide to antibody. Purification was carried out using Sepharose CL-4B gel filtration columns. RNA content was calculated by performing a modified Quant-iT RiboGreen RNA assay. After addition of the targeting ligand, all the targeted and non-targeted LNP preparations were kept at 4 °C and were used within three days of preparation.

2.5. cicrRNA synthesis and encapsulation in LNPs

The EBNA1 CAR construct contained the EBNA1 peptide (EAD YFEYHQEGGPDGEFHPVGDADYFEY) with mouse CD3ζ and 4-1BB cytoplasmic signalling domains. CAR expression circRNA was synthesized and supplied by GENESEED. The circRNA was analyzed by agarose gel electrophoresis and was stored at −80 °C. Purified circRNA was encapsulated in LNP using a self-assembly process with microfluidic as previously described[23]. Briefly, the organic phase consisted of ethanol containing dissolved ionizable lipid, auxiliary lipids, cholesterol, and polyethylene glycol lipid, while the aqueous phase contained circRNA dissolved in citrate buffer. The aqueous and organic phases were mixed in a 3:1 ratio within a microfluidic chip device using syringe pumps, the total flow rate was 0.8 mL/min. The formulated LNPs were subsequently dialyzed against PBS (pH 7.4) for ethanol removal.

2.6. The nucleotide sequence of CAR

UACCGGAAUGGTCACUGGCGGAACGAGGACGGCGACCG
GAACGACGAGGTGCGGCGGUCCGGCCUCGUCUUUGAGU
AGAGACUUCUCCUAGACUCGGUCUCGUCGUCGUCGCCG
UCGGGGGGGUCCUCCGGGGGGGGGCCGUCCUCCGGGA
AGAAGGUGGGGCACCCGCUGCGGCUGAUGAAGCUCAUG
UGGUGCUGCGGUCGCGGCGCUGGUGGUUGUGGCCGCG
GGUGGUAGCGCAGCGUCGGGGACAGGGACGCGGGUCUC
CGCACGGCCGGUCGCCGCCCCCCGCGUCACGUGUGCUC
CCCCGACCUGAAGCGGACACUAUAGAUGUAGACCCGCG
GGAACCGGCCCUGAACACCCCAGGAAGAGGACAGUGAC
CAAUAGUGGGAAAUGACGUUUGCCCCGUCUUUCUUUG
AGGACAUAUAUAAGUUUGUUGGUAAAUACUCUGGUCAU
GUUUGAUGAGUUCUCCUUCUACCGACAUCGACGGCUAA
AGGUCUUCUUCUUCUUCCUCCUACACUUGACUCUCACU
UCAAGUCGUCCUCGCGUCUGCGGGGGCGCAUGGUCGUC
CCGGUCUUGGUCGAGAUAUUGCUCGAGUUAGAUCCUGC
UUCUCUCCUCAUGCUACAAAACCUGUUCUCUGCACCGG
CCCUGGGACUCUACCCCCCUUUCGGCGUCUCUUCCUUC
UUGGGAGUCCUUCCGGACAUGUUACUUGACGUCUUUCU
AUUCUACCUCCUCCGGAUGUCACUCUAACCCUACUUUC
CGCUCGCGGCCUCCCCGUUCCCCGUGCUACCGGAAAUG
GUCCCAGACUCAUGUCGGUGGUUCCUGUGGAUGCUGCG
GGAAGUGUACGUCCGGGACGGGGGAGCG (from 5′ to 3′).

2.7. Nanoparticle characterization

The targeted and non-targeted particles were characterized by NanoSight NS300 instrument (Malvern Instruments, Malvern, UK) for number, average hydrodynamic radius, and concentration. The zeta potential of the particles was determined using a ZetaPALS Zeta Potential Analyzer (Brookhaven Instruments Corporation, Holtsville, NY, USA). Samples were imaged with a JEOL JEM-1400 transmission electron microscope operating at 120 kV (JEOL USA, Peabody, MA, USA).

Encapsulation Efficiency (EE) were calculated using Quant-iT RiboGreen assays (Thermo Fisher Scientific). The Quant-iT RiboGreen RNA kit was mixed with LNP or LNP demulsified with 2% Triton X-100. With excitation by a laser at 480 nm, the fluorescence intensity at 520 nm was detected by a multimode plate reader (EnSight, PerkinElmer, Singapore), and the cirRNA content was calculated according to the standard curve. The circRNA contents were measured using the following Eq. (1):

$$\mathrm{EE}\ (\%) = (m2\text{-}m1)/m2 \times 100 \quad (1)$$

Where $m1$ is the weight of LNP before demulsification using 2% Triton X-100, $m2$ is the weight of LNP after demulsification using 2% Triton X-100.

2.8. *In vitro cytotoxicity assay*

For cytotoxicity assays, primary T cells and the T-cell line CTLL-2 cells were seeded in 96-well plates (5×10^3 cells/well) and treated with CD7/LNP for 24 h, with circRNA concentrations ranging from 100 to 1000 ng/mL. And cell viability was quantified using a CCK-8 kit according to the manufacturer's instructions.

2.9. *Confocal microscopy*

For confocal laser scanning microscopy (CLSM) observations, primary T cells and CD7/LNP were cultured at 37 °C for 2 and 8 h, respectively. The nuclei and lysosomes/endosomes were stained with DAPI and LysoTracker dyes respectively. To evaluate the cellular uptake of each circRNA formulation, free cirRNA and CD7/LNP were incubated with CTLL-2 and primary T cells for 4 h, respectively. Then, the cells were washed three times with PBS and transferred onto fibronectin-coated 10-mm Teflon ring glass slides, fixed in 2% paraformaldehyde, mounted with ProLong Gold Antifade reagent for 24 h, and imaged with a Zeiss LSM 780 confocal microscope.

2.10. *In vitro T-cell transfection using CD7/LNP*

Mice were euthanized using carbon dioxide anesthesia and then immersed in 75% alcohol for processing. Remove the spleen, and place in separate 15 mL tubes containing 5 mL ice-cold RPMI/FBS (RPMI with 2% FBS). Next using the plunger of a 1 mL syringe, mash the spleen using a 40 μm filter until it has been torn into very fine parts to generate a single cell suspension. Transfer the cell suspension to a 15 mL tube, and spin down at $400 \times g$ for 5 min at 4 °C for removing the supernatant. After pelleting the cells and removing the supernatant, re-suspend the cells with 1 mL RBC lysis buffer for every 10^8 cells for 3−4 min. Stop RBC lysis with 14 mL ice-cold PBS and spin down at $400 \times g$ for 5 min at 4 °C. Afterwards, mouse spleen T cells were sorted using a mouse T cell magnetic beads separation kit. Purified T cells can be obtained by performing the sorting steps according to the protocol in the kit.

T cells were activated using CD3/CD28 Dynabeads (Gibco 11453D), expanded using 100 Units/mL of recombinant mouse interleukin-2 (R&D Systems 402-ML) and grown in RPMI 1640 (Invitrogen 11875085) containing 10% FBS (Atlanta Biologicals S11150), 4 mmol/L L-glutamine (Invitrogen 25030081), penicillin/streptomycin (Invitrogen 15140122), 1 mmol/L sodium pyruvate (Invitrogen 11360079), and 50 μmol/L 2-mercaptoethanol (Gibco 21985023). Subsequently, activated T cells were plated and cultured with the nanoparticle suspension, using the CD7/LNP concentrations as indicated. Transfection efficacy was evaluated by flow cytometry 48 h later.

2.11. *Generation of EBNA1 CAR-T cells with LNP*

T cells were sorted and activated above. After 6−8 days of activation, T cells are in a resting state and further expansion of T cells requires a restimulation. Finally, the isolated and activated T cells were coincubated with LNP to construct EBNA1-CAR T cell.

2.12. *Lentiviral production and ex vivo T cell transduction*

Lentiviral stocks were generated by transfection of 293T cells with the pLenti-CAR-IRES-GFP, psPAX2 and pMD2.G plasmids followed by concentration as previously reported[24]. For lentiviral gene transfer into murine T cells, 1 mL per well of lentivirus was preloaded on six-well non-tissue culture treated dishes coated with RetroNectin and incubated at 37 °C for 1 h. An equal volume of Concavalin A/IL-7 activated T lymphocytes (3×10^6 cells/mL in RPMI medium supplemented with 100 Units/mL of recombinant mouse IL-2) was added and centrifuged at $2000 \times g$ for 30 min. Six h after spinoculation, 1 mL of fresh, prewarmed RPMI containing 50 IU IL-2 was added. T cells were used for adoptive transfer experiments 2 days after gene transfer.

2.13. *Detection of CAR expression*

The primary anti-MYC (1:1000, Abcam, ab32) antibodies were used for Western blotting for CAR protein expression detection, performed using to an established method. Further, FITC labeled EBNA1 antibody was used to detect the CAR expression on T cell surface.

2.14. *Functional in vitro T cell assays*

2.14.1. *In vitro killing assay*

We measured *in vitro* cytotoxic activity of CAR-T cells using standard LDH assay as described elsewhere[25]. Briefly, T cells and targeted cells were added to the suspensions at varying effector-to-target cell ratios in 96-well plates (final volume, 200 μL) and incubated for 6 h at 37 °C. Then, cell death was assessed by LDH Cytotoxicity Assay Kit.

2.14.2. *Cytokine secretion assay*

Supernatants were collected and stored at −80 °C until use in this assay and were thawed on ice upon use. T cell cytokine release was measured with ELISA kit[26].

2.15. *Nanoparticle biodistribution and toxicity studies*

The mice were intravenously injected with Cy5-tagged nanoparticles (at the dosage of 0.5 mg circRNA/kg) that were either non-targeted, or targeted. The nanoparticle suspension was administered through a tail vein as described above. After 6 h, tissues as indicated were removed, weighed, and macerated as needed with scissors. We quantified specific Cy5 tissue fluorescence for each organ using the IVIS Spectrum imaging system.

To measure potential *in vivo* toxicities of repeatedly infusing lymphocyte-targeted RNA nanocarriers, CD7-targeted nanoparticles carrying EBNA1 CAR-encoding circRNA (at the dosage of 0.5 mg circRNA/kg) were intravenously injected every other day as previously reported[27]. Control animals received no treatment. Forty-eight hours after the final nanoparticle infusion, mice were anesthetized and blood was collected into serum separator tubes for serum chemistry and cytokine profile analyses. Animals were then euthanized with carbon dioxide to retrieve organs, which were washed with deionized water before fixation in 4% paraformaldehyde. The tissues were processed routinely, and sections were stained with haematoxilin and eosin.

2.16. *B cell detection*

B cells after treatment were measured with flow cytometry (EBNA1 Protein, ACRO Biosystems and PE Streptavidin, Biolegend) or ELISpot as described elsewhere. For ELISpot assay, peripheral blood-derived B cells from different treated mouse were isolated with B cell negative isolation Kit and suspended in

ELISpot wells incubated with 5 μg/mL of EBNA1 peptide, 5 μg/mL of bovine serum albumin (BSA) or 15 μg/mL of mouse total IgG monoclonal antibody. After incubation in ELISpot plates for 18 h, plates were washed, developed using TMB substrate, and quantitated using a Bio-Reader system (BioSys).

2.17. T cell detection with flow cytometry

Mice were sacrificed, and spinal cords were isolated, treated with 0.5 mg/mL DNase and 1 mg/mL Liberase for 30 min at 37 °C, homogenized and strained through a nylon filter with a pore size of 100 μm. Viable immune cells were collected and washed extensively before being stained. For flow cytometry, cell surface antibodies were first incubated with the cells for 20 min at 4 °C. T cell were tested using the following panel of antibodies: anti-CD45, anti-CD3, PE-Labeled Mouse H-2 Tetramer-EADYFEYHQ EGGPDGE and LIVE/DEAD™ Fixable Lime (506) Viability Kit.

2.18. Histology and immunofluorescence staining

At the time of sacrifice, mice were transcardially perfused with 4% paraformaldehyde. Spinal cords were removed and fixed in the same fixative for 24 h. They were washed using PBS and embedded in OCT in cryomoulds. Sections were cut at 8-μm thickness using a cryostat. Luxol fast blue (LFB) staining was used to evaluate myelin differentiation. Spinal cord and brain sections were desiccated for 1 h and then subjected to a series of washing steps with ethanol, lithium carbonate, Harris haematoxylin, acid alcohol, ammonium hydroxide, and eosin Y. For LFB, 3 different animals were examined, with at least 10 sections per animal. All spinal cord slides were analysed using a Nikon system.

For T cell detection, samples were incubated with 10% normal goat serum or 0.5% Triton in PBS for 1 h at RT, dried, incubated with a primary antibody against CD3 (1:500 dilution, *v*/*v*) and placed in a 4 °C room overnight. The samples were then washed 3 times with PBS for 5 min and incubated with secondary antibodies for 1 h at RT. The following secondary antibodies were used: Alexa Fluor 488 goat anti-rabbit IgG and Alexa Fluor 594 goat anti-hamster IgG. After washing with PBS 3 times for 5 min, the samples were mounted with DAPI. The slides were finally analysed using a Nikon microscope.

Nissl staining was used to evaluate the neuronal status after treatment. Nissl staining was performed on transverse sections rostral to the epicentre with 0.1% cresyl violet for 20 min at 37 °C. After the samples were rinsed with distilled water, the stained sections were differentiated in 95% ethyl alcohol. Then, the sections were dehydrated with increasing concentrations of ethyl alcohol and cleared using xylene. The quantitative analysis of Nissl bodies and the neuronal status was performed using multiple sections from at least three different spinal cord regions from three animals. All spinal cord slides were analysed using a Nikon system.

2.19. In vivo anti-Staphylococcus aureus efficacy assay

After the treatment with CD7/LNP and CD19 Ab, the mice were injected (i.p.) with *Staphylococcus aureus* (SA, 1×10^8 CFU/mouse, 100 μL), body weight and probability of survival were statistically analyzed. After 24 h of infection, peripheral bloods from the live mice were collected and inoculated on SDA medium. Then the SA CFUs were quantified. The levels of cytokines, including IL-4, TNF-α, and IL-10, in the serum were determined by ELISA following the instructions recommended by the manufacturer.

2.20. Statistical analysis

Differences between two conditions were assessed using Students *t*-test. Significance was determined for multiple conditions using one-way analysis of variance (ANOVA). Significant ANOVA results ($P < 0.05$) were analyzed further using Tukey's *post hoc* multiple comparisons test. All results are presented as mean ± standard deviation (SD). All graphs were generated using Prism 8.0 software (GraphPad Software, Inc., San Diego, CA, USA).

3. Results

3.1. Synthesis and characterization of the CD7-targeted LNPs

To precisely and efficaciously program T cells, we first designed an ionizable lipid nanomaterial (Supporting Information Scheme S1, Figs. S4−S7) and copackaged EBNA1-CAR circRNA (Supporting Information Fig. S8) into lipid nanoparticles (LNPs) by microfluidic self-assembly, in which the T cells-targeting CD7 antibody was coupled to the surface of LNPs (Fig. 1B). The LNPs were formed and screened according to transfection efficiency, fabricated with the following molar ratios of ionizable lipid (35):cholesterol (46.5):DOPE (16):DMG-PEG-Mal (2.5) (Supporting Information Fig. S9), then modified with CD7 antibodies (CD7/LNP). As shown in Fig. 1C−E, the synthesized LNP exhibited a spherical morphology with a 122.6 ± 4.7 nm hydrodynamic size distribution, and their ζ potential was −0.193 ± 0.61 mV, the synthesized CD7/LNP exhibited a spherical morphology with a 144.3 ± 8.3 nm hydrodynamic size distribution, and their ζ potential was −1.08 ± 0.21 mV. And the encapsulation efficiency (EE) of the circRNA was 86.4 ± 0.7% (Supporting Information Fig. S10). To determine the cytotoxicity of CD7/LNP, primary T cells, and the T-cell line CTLL-2 cells were treated with CD7/LNP for 24 h, compared to a phosphate-buffered saline (PBS)-treated group, and no significant difference in viability was observed (Fig. 1F and Supporting Information Fig. S11). Further, the stability of CD7/LNP was evaluated according to hydrodynamic size distribution and PDI. As shown in Fig. 1G, CD7/LNP were stable in PBS, with negligible size and PDI differences, for 7 days at 4 °C, which indicated that the CD7/LNP have excellent stability. Collectively, these results indicate that the CD7/LNP had the potential to mediate gene delivery.

To evaluate the immunogenicity of CD7/LNP, CD7/LNP was administered to WT mice, and blood samples were collected to measure immunogenicity assessment related cytokines (IL-6, TNF-α, and IFN-γ) and anti-PEG IgM levels in plasma at Days 0, 2, 4 and 7. As shown in Fig. 1H and I, immunogenicity assessment related cytokines peaked on Day 1 and serum anti-PEG IgM levels peaked on Day 2 both returned to baseline by Day 7. Further, Human PBMCs were exposed to CD7/LNP for 6 h, CD69 and CD107 expression were detected to determine the potential immunogenicity of CD7/LNP on human. Supporting Information Fig. S12 shows no significant CD69 and CD107 were detected in CD7/LNP and LNP treated groups. Together, these data indicate that CD7/LNP can be loaded with circRNA for T cells programming with low immunogenicity.

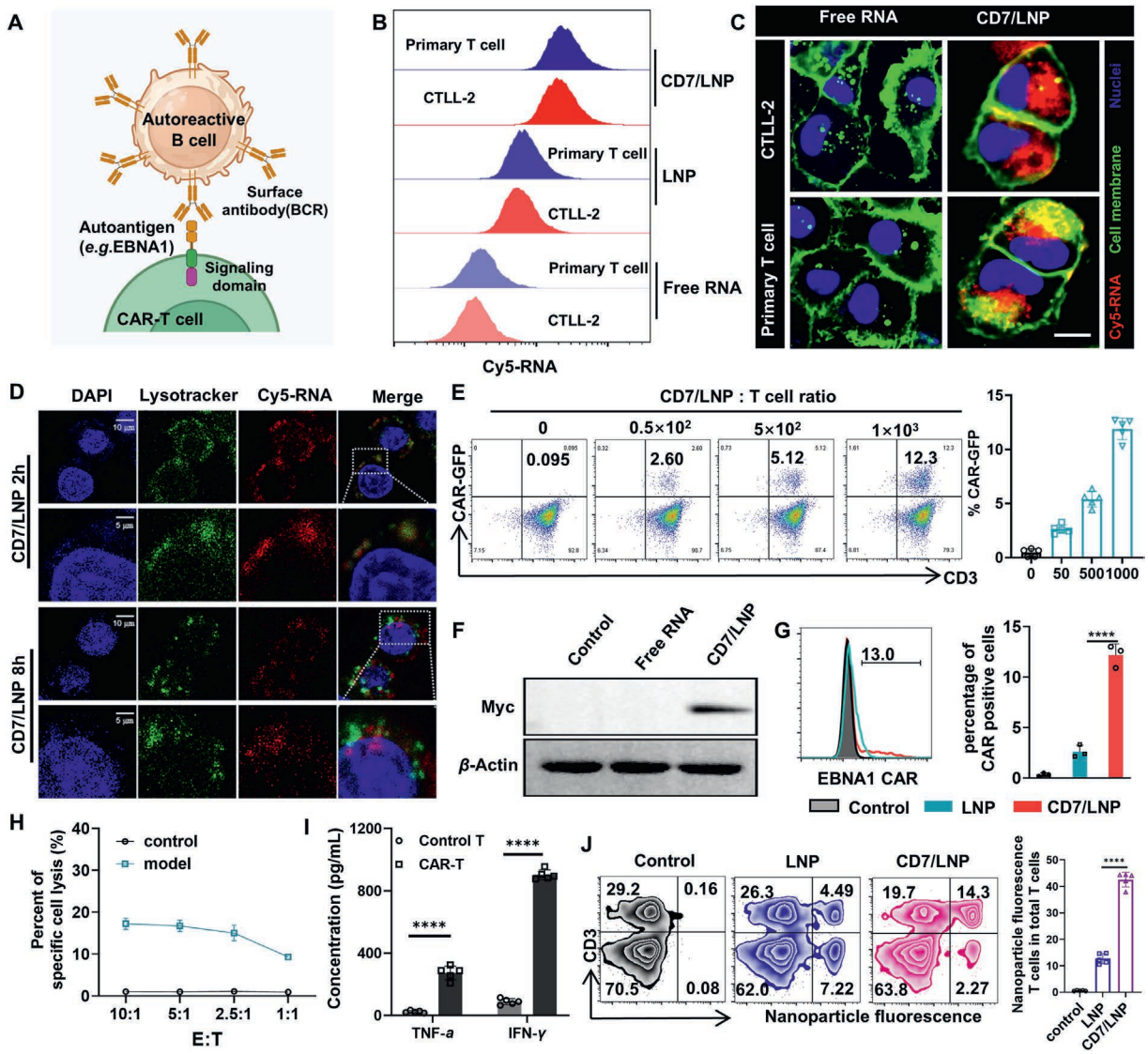

Figure 2 CAR expression and effector activity of CAR-T cells *in vitro*. (A) Design of EBNA1 CAR. (B) Free circRNA and LNP with or without CD7 were cocultured with CTLL-2 and primary T cells for 4 h, cellular uptake of free circRNA and LNP with or without CD7 by CTLL-2 and primary T cells was evaluated by FC analysis. (C) Confocal images of CTLL-2 and primary T cells treated with free circRNA or CD7/LNP for 4 h. The cell membrane and nuclei were counterstained with WGA (green) and DAPI (blue), respectively. Scale bars = 10 μm. (D) Confocal images of subcellular compartments of primary T cells after coincubation with LNP or CD7/LNP. Images from left to right show DAPI-stained cell nuclei (blue), lysosomes (green), circRNA (red), and merged images. Scale bars = 20 μm. (E) Primary T cells were treated with CD7/LNP at LNP/T cell number ratio from 50:1 to 1000:1 for 24 h, percentage of GFP-positive T cells was detected by flow cytometry analysis (n = 5 cell samples per group, biological replicates). (F) Abundance of the EBNA1 protein in T cells after treatment with CD7/LNP at the LNP/T cell ratio of 1000:1 or relatively equivalent quality free RNA was detected with Western blot. (G) Primary T cells were treated with CD7/LNP or LNP at the LNP/T cell ratio of 1000:1, expression of EBNA1 on the cell surface was detected with flow cytometry analysis (n = 3 cell samples per group, biological replicates). Data are presented as mean ± SD. ****$P < 0.0001$ *vs.* indicated. (H, I) Effector cells, sorted CAR-T cells; target cells, freshly sorted B cells from WT (control) and EAE mice (model). After coculture at the indicated ratios for 8 h, the percentage of lysed B cells (H) and the supernatant TNF-α and IFN-γ concentrations (I) after 8 h of coculture at the ratio of 10:1 were analyzed by CCK-8 and ELISA respectively (n = 5 cell samples per group, biological replicates). Data are presented as mean ± SD. ***$P < 0.001$, ****$P < 0.0001$ *vs.* indicated. Statistical significance was analyzed using one-way ANOVA (E, H) and two-way ANOVA (J). (J) Mouse spleen lymphocytes were sorted and cultured with nontargeted LNPs or targeted LNPs for 4 h, and nanoparticle fluorescence on T cells was detected by flow cytometry analysis (n = 5 cell samples per group, biological replicates). Data are presented as mean ± SD. ****$P < 0.0001$ *vs.* indicated.

3.2. CD7-targeted LNPs produce functional, circRNA-based CAR-T cells in vitro

The efficiency of LNP-mediated gene delivery was tested with primary T cells and the T-cell line CTLL-2, which allows T cells to express corresponding CAR proteins, including the CD8α hinger and 4-1BB transmembrane domains, the CD3ζ intracellular signaling domain, and the EBNA1 extracellular domain (Fig. 2A). Flow cytometry results (Fig. 2B) and confocal imaging (Fig. 2C) established that in both primary T cells and T-cell lines, substantial enhancement was achieved in the cellular internalization of genes after encapsulation in CD7-targeted LNPs *in vitro*. The quantitative results of flow cytometry fluorescence intensity showed that the intracellular RNA fluorescence intensity in the CD7/LNP group was 11.3 times higher than that of free RNA. These results indicated that the LNPs efficiently delivered the genes into T cells with the CD7 motif, presumably as a result of receptor-induced endocytosis. As the incubation time extended to 8 h, the wide distribution of Cy5-circRNA in the cytoplasm of T cells indicated that the LNPs escaped the lysosome and entered the cytosol, which further upregulated CAR protein expression (Fig. 2D, Supporting Information Fig. S13).

We then assessed the ability of the engineered nanoparticles to program T cells by incubating freshly isolated, activated murine T cells with the particles at various ratios *in vitro* for 48 h. With GFP as a marker of CAR, the expression of CAR was evaluated by FC, and the expression level increased with the increase in the ratio of nanoparticles to cells, indicating that nanoparticles mediate T-cell programming (Fig. 2E). Next, we tested CAR expression on the cell surface of the treated cells. After incubation with CD7/LNP, Myc and EBNA1 in T cells were measured using Western blot analysis (Fig. 2F) and flow cytometry (Fig. 2G), respectively. As shown in Fig. 2G, in the CD7/LNP treatment group, the percentage of EBNA1-positive T cells was 12.2 $\pm$ 1.12%, considerably higher than that of the EBNA1/LNP-treated cells. These results provided direct evidence that CD7/LNP drove the successful expression of CAR on the T-cell surface. Also, human Jurkart cell and T cells isolated from human PBMCs were cocultured with CD7/LNP for 48 h. As shown in Supporting Information Fig. S14, the average transfection efficiency was 50.2% in Jurkart cell (Fig. S14A) and 11.2% in human primary T cell (Fig. S14B), indicating that it can be used for human T cell transfection.

Then, Live GFP$^+$ T cells were sorted by FACS as EBNA1 CAR-T cells, and their specific killing ability toward anti-EBNA1 B cells was tested by coincubating EBNA1 CAR-T cells with primary B cells from EAE mice and WT mice. The LNP transduced CAR-T cells showed compared specific killing efficacy with lentivirally transduced CAR-T cells to B cells from EBNA1 induced EAE mice and nearly no killing efficacy to B cells from WT mice (Fig. 2H, Supporting Information Fig. S15). Enzyme-linked immunosorbent assay (ELISA) and FC detection revealed substantial T-cell effector molecule IFN-γ, TNF-α secretion by the CAR-T cells after their coculture with the target cells (Fig. 2I).

We also assessed the ability of CD7/LNP to program specificities against T cells by incubating mouse splenocytes with the particles. We found that CD7-targeted nanoparticles selectively bound T lymphocytes, and their interactions with off-target cells were low (Fig. 2J). CD7/LNP-transfected T cells exhibited certain enhanced cytotoxic activity against EAE mouse derived B-cell compared to standard LNP-transfected cell (Supporting Information Fig. S16A), accompanied by markedly elevated secretion of key effector molecules (Fig. S16B) including IFN-γ and TNF-α. We further quantitatively analyzed the ratios of CD4$^+$ T cells, CD8$^+$ T cells, and NK cells after co-incubation with CD7/LNP. Flow cytometry results showed that the uptake rates for CD8$^+$ and CD4$^+$ T cells were approximately 29.9% and 62.9%, respectively, while NK cells had an uptake rate of 7.19% (Supporting Information Fig. S17). The uptake results of CD8$^+$ and CD4$^+$ T cells were consistent with the CAR expressing results, possibly due to CD7-mediated targeted endocytosis, which further enabled effective gene expression. And we quantified the CAR expression in CD8$^+$, CD4$^+$ T cells and Treg cells. As shown in Supporting Information Fig. S18, the percentage of CAR expressing T cells with respect to CD8$^+$, CD4$^+$ T cells and Treg cells was 32.5 $\pm$ 0.66%, 46.8 $\pm$ 0.85% and 0.96 $\pm$ 0.085%, respectively. These data suggested that CD7/LNP could specifically target T cells and that LNP-engineered CAR-T cells had increased cytotoxicity against anti-EBNA1 B cells but no cytotoxicity against normal B cells, providing support for further translation of this strategy for T-cell reprogramming *in vivo*.

3.3. CD7-targeted LNPs facilitate the generation of CAR-T cells in vivo

To determine whether the targeted nanoparticles can specifically reprogram circulating T cells with EBNA1-CAR genes *in situ*, we intravenously injected CD7-targeted LNPs and examined how exclusively CD7-mediated targeting confined nanoparticle interactions with circulating T cells. FC analysis of peripheral blood collected 4 h later established that 12.7 $\pm$ 2.0% of the circulating T lymphocytes bound CD7-targeted nanoparticles, while signals from off-target cells in peripheral blood were low (Fig. 3A and B).

In parallel experiments, we quantified the distribution of nanoparticles in various organs 4 h after intravenous injection. The highest concentrations of nontargeted particles were found in the liver, while lymphocyte-targeted nanocarriers accumulated mainly in the spleen and liver (Fig. 3C). No hepatotoxicity or nephrotoxicity was detected, and no breathing problems or weight loss were observed (Supporting Information Fig. S19).

To determine if the targeted nanoparticles can reprogram circulating T cells with EBNA1-CAR genes *in situ*, CAR expression on circulating T cells was dynamically detected and verified during 10 days of detection. The long-term expression of CAR protein *in vivo* may be related to the stability of circRNA. The proportion of EBNA1 CAR-T cells was the highest on the second day, accounting for approximately 4.7% of peripheral lymphocytes (Fig. 3D and E), CAR-T cells were detectable in peripheral blood at 10 days and declined to baseline by Day 14. Furthermore, a more detailed phenotypic analysis on Day 2 (Fig. 3F, Supporting Information Fig. S20) and Day 7 (Supporting Information Fig. S21) revealed that the GFP$^+$ cells in peripheral blood were mainly expressed in T cells, and a small amount was expressed in neutrophils and macrophages, which further indicated that CD7/LNP specifically targeted and programmed T cells *in vivo*.

Further, to detect long term persistence of CAR-T cells, GFP$^+$ cells from mice injected with CD7/LNP were sorted at Days 2, 4 and 8, and co-incubated with primary B cells from EAE mice for 8 h at the effect target ratio of 10:1. Killing ability and T-cell effector molecule IFN-γ secretion were detected, as shown in Fig. 3G and H, CAR-T cells sorted from Days 2, 4 and 8 exhibit comparable cytotoxicity to autoimmune B cells, indicating functional persistence of CAR-T cells. Meanwhile, PD1, TIM3 and LAG3 expression on GFP$^+$ cells were detected to evaluate potential exhaustion of CAR-T cells. While PD-1 expression increased modestly over time

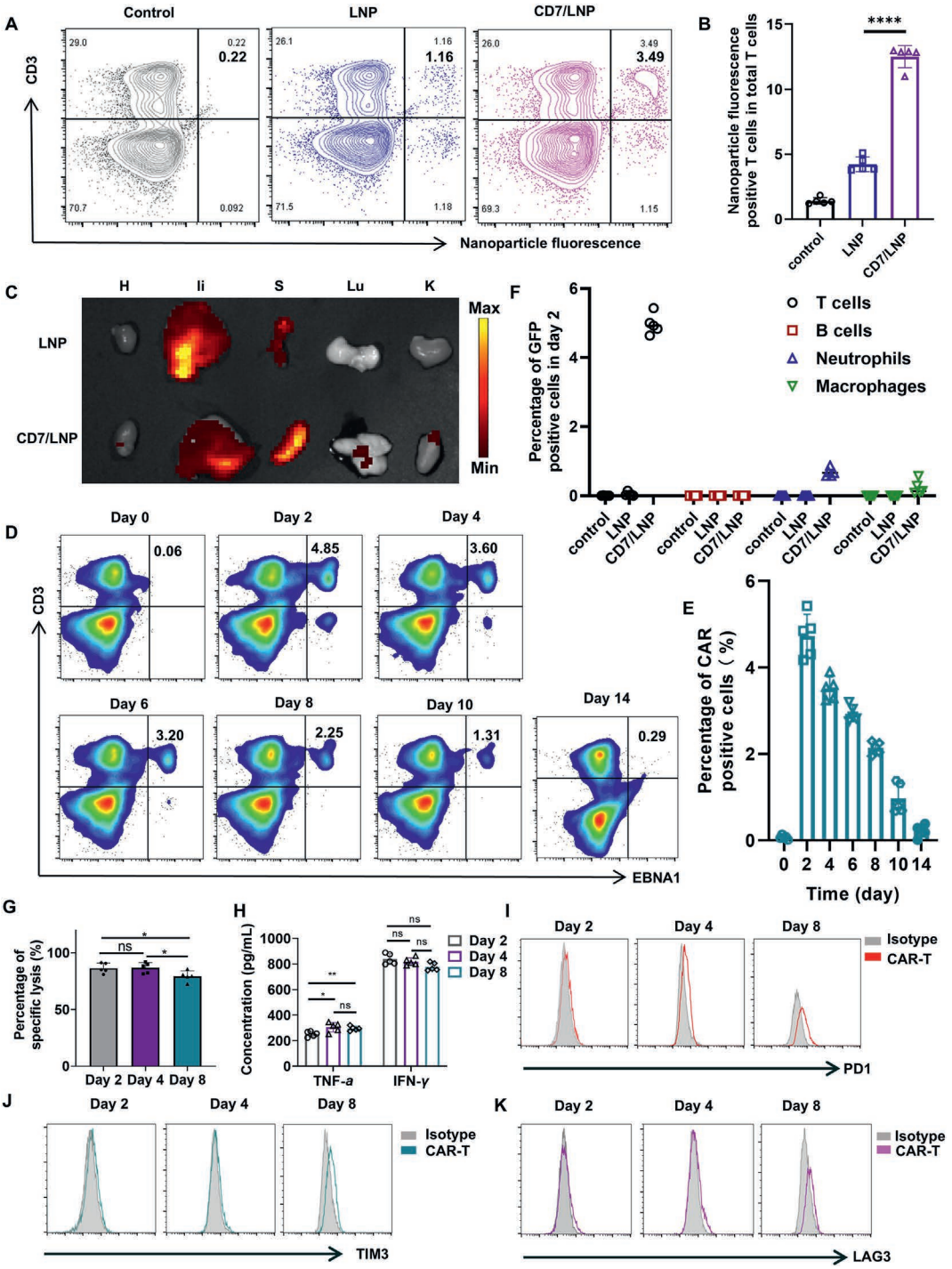

Figure 3 CD7-targeted LNPs bind to circulating T cells and produce CAR-T cells *in vivo*. (A, B) Flow cytometry demonstrating fluorescent nanoparticle binding to peripheral T cells 4 h after injection ($n = 5$ mice per group, biological replicates). Data are presented as mean ± SD, $^{****}P < 0.0001$ *vs*. indicated. (C) Bioluminescent imaging of nanoparticle distributions 24 h after tail vein injection with CD7-targeted LNPs or nontargeted nanoparticles (H for heart, Li for liver, S for spleen, Lu for lung, K for kidney). (D, E) Reprogramming host T cells with EBNA1-CAR genes. CD7/LNP was administered to WT mice, CAR expression was detected for 14 days post-injection by flow cytometry (D) and quantified (E) ($n = 5$ mice per group, biological replicates). (F) Quantification of GFP-positive macrophages, neutrophils, T cells and B cells in peripheral blood after the injection of LNP or CD7/LNP at day 2 ($n = 5$ mice per group, biological replicates). (G−K) Long-term persistence and potential exhaustion of CAR-T cells. GFP^+ cells were sorted on Days 2, 4 and 8, and co-incubated with EBNA1 specific B cells for 8 h at the effect target ratio of 10:1. Killing ability (G) and T-cell effector molecule TNF-α, IFN-γ secretion (H) were detected by LDH assay and ELISA respectively. Also, expression of PD1 (I), TIM3 (J) and LAG3 (K) on GFP^+ cells sorted at Days 2, 4 and 8 were detected to evaluate potential exhaustion of CAR-T cells by flow cytometry. One-way ANOVA with Tukey's HSD test were used to determine P values ($n = 5$ mice per group, biological replicates). Data are presented as mean ± SD, $^{*}P < 0.05$, $^{**}P < 0.01$ *vs*. indicated; ns, not significant.

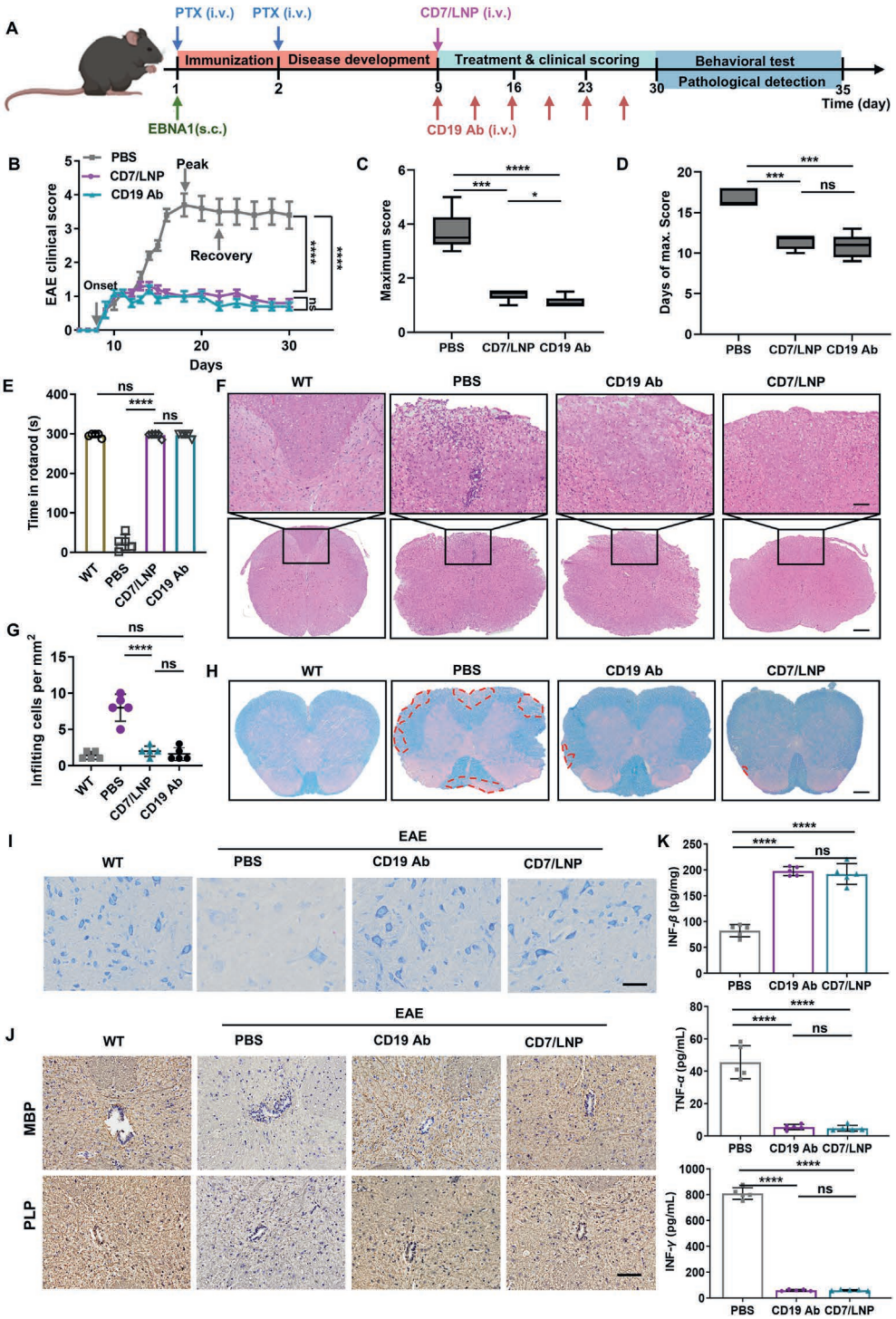

Figure 4 Modulation of EAE in mice by intravenously delivered CD7/LNP. (A) Schematic representation of the procedure used to induce EAE and the treatment that the mice received on Day 9, followed by clinical scoring until Day 30. PTX (pertussis toxin). (B) Changes in the clinical scores of EAE mice immunized with EBNA1 peptide and treated with PBS, CD7/LNP or CD19 Ab starting on Day 9 ($n = 5$ mice in all groups). Arrows represent timepoints of EAE onset peak and recovery. Data are presented as mean ± SD, $^{*}P < 0.05$, $^{****}P < 0.0001$ *vs.* indicated. (C) Maximum disease score of different treat mouse ($n = 5$ mice per group, biological replicates). Data are presented as mean ± SD.$^{*}P < 0.05$, $^{***}P < 0.001$, $^{****}P < 0.0001$ *vs.* indicated. (D) Day of onset of maximum score of different treatment groups of mice ($n = 5$ mice per group, biological replicates). Statistical significance was analyzed using one-way ANOVA. Data are presented as mean ± SD, $^{***}P < 0.001$; ns, not significant. ns, not significant. (E) Rotarod assessment of sensorimotor processes in the different groups ($n = 5$ mice per group, biological replicates). Statistical significance was analyzed using one-way ANOVA. Data are presented as mean ± SD, $^{****}P < 0.0001$ *vs.* indicated; ns, not significant. (F) Representative images of H&E staining of the spinal cords from WT mice, untreated and treated mice in B. Scale bar: 500 μm (top panel), 100 μm (bottom panel). (G) Inflammatory infiltrating cells per mm^2 from lumbar spinal cord sections from F ($n = 5$ mice per group,

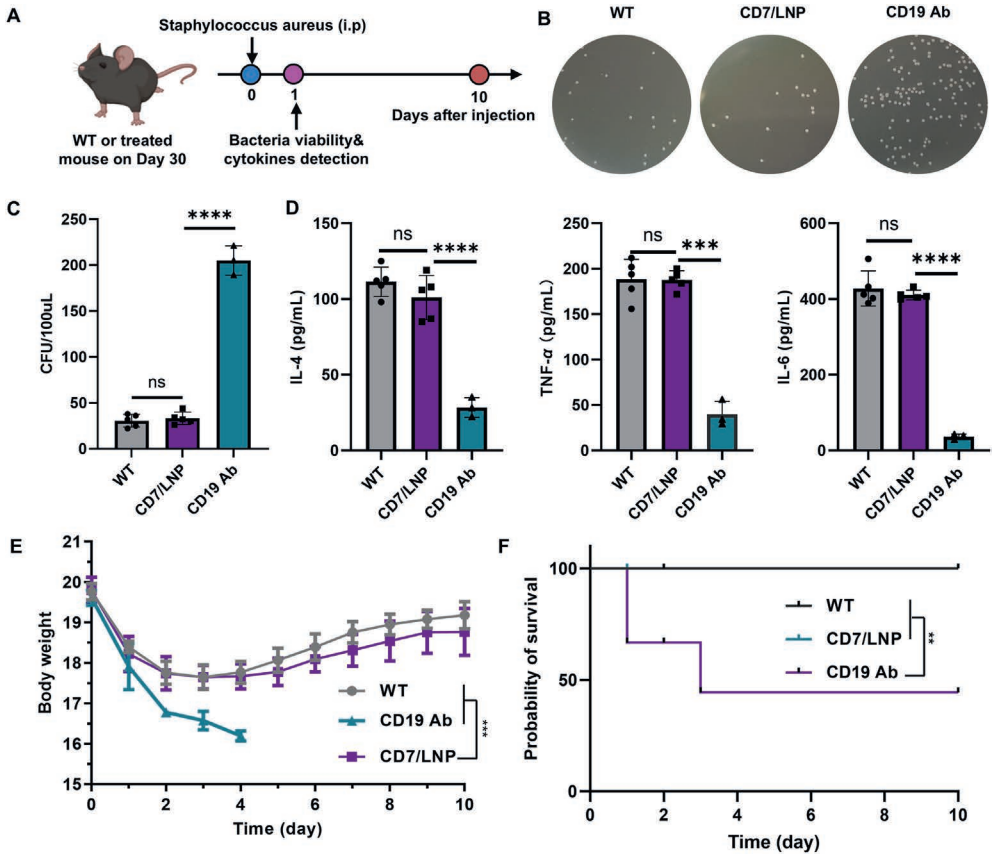

Figure 5 EBNA1-specific B-cell depletion by CD7-targeted LNPs avoids the risk of infection caused by total B-cell depletion. (A) Scheme of the mouse model injected with *Staphylococcus aureus* to evaluate their immune response. (B) Representative images showing the bactericidal activity of B cells with the indicated treatment. (C) Bacterial CFU counts per 100 μL from mice infected with *Staphylococcus aureus* ($n = 5$ mice per group, biological replicates). Data are presented as mean ± SD, $^{****}P < 0.0001$ *vs*. indicated; ns, not significant. (D) Concentration of IL-4, TNF-α and IL-6 secreted by differently treated mice ($n = 5$ mice per group, biological replicates). Statistical significance was analyzed using one-way ANOVA. Data are presented as mean ± SD, $^{***}P < 0.001$, $^{****}P < 0.0001$ *vs*. indicated; ns, not significant. (E) The body weight of the mice ($n = 5$ mice per group, biological replicates, the absence of mice in certain treatment groups is due to the failure of infected mice to survive until the sampling time point). Data are presented as mean ± SD, $^{***}P < 0.001$ *vs*. indicated. (F) Percentage survival of mice after bacteria injection ($n = 5$ mice per group, biological replicates). Statistical significance was analyzed using one-way ANOVA. Data are presented as mean ± SD, $^{**}P < 0.01$ *vs*. indicated.

(Fig. 3I–K), CAR-T cells retained functional cytotoxicity and cytokine secretion even at late timepoints (Fig. 3G and H), suggesting that transient exhaustion does not compromise therapeutic efficacy. These data demonstrate that CD7/LNP-generated CAR-T cells maintained functional persistence for at least 7 days while avoiding chronic exhaustion risks, supporting their suitability for autoimmune therapy. Also, the majority of *in situ*-generated CAR-T cells exhibit an effector memory phenotype (Supporting Information Fig. S22).

3.4. CD7-targeted LNPs-mediated EBNA1-specific B-cell depletion modulates EAE in mice but avoids the risk of infection caused by total B-cell depletion

Next, we sought to examine the therapeutic effect of CD7/LNP on the-established EAE model mice as descripted. Approximately 9 days after model construction the mice began to show extensive symptoms of MS, then the mice were divided into different groups and injected with CD7/LNP or 1D3 antibodies (CD19 ab) to start

biological replicates). Statistical significance was analyzed using one-way ANOVA. Data are presented as mean ± SD, $^{****}P < 0.0001$ *vs*. indicated; ns, not significant. (H) Representative spinal cord sections stained with LFB. Dashed lines indicate areas of white matter damage. Scale bar = 500 μm. (I) Images of Nissl staining in the spinal cords of WT mice and EAE mice after treatment with PBS and different preparations. Scale bar = 100 μm. (J) Representative antimyelin basic protein (MBP and PLP) staining the spinal cords of WT mice and EAE mice after treatment with PBS and different preparations, revealing areas of the degree of myelin injury. Scale bar = 100 μm. (K) Cytokine profiles in spinal cords of different treated mouse were analysed using ELISA ($n = 5$ mice per group, biological replicates). One-way ANOVA with Tukey's HSD test was used to determine P values. Data are presented as mean ± SD, $^{*}P < 0.05$, $^{**}P < 0.01$, $^{***}P < 0.0001$ *vs*. indicated; ns, not significant.

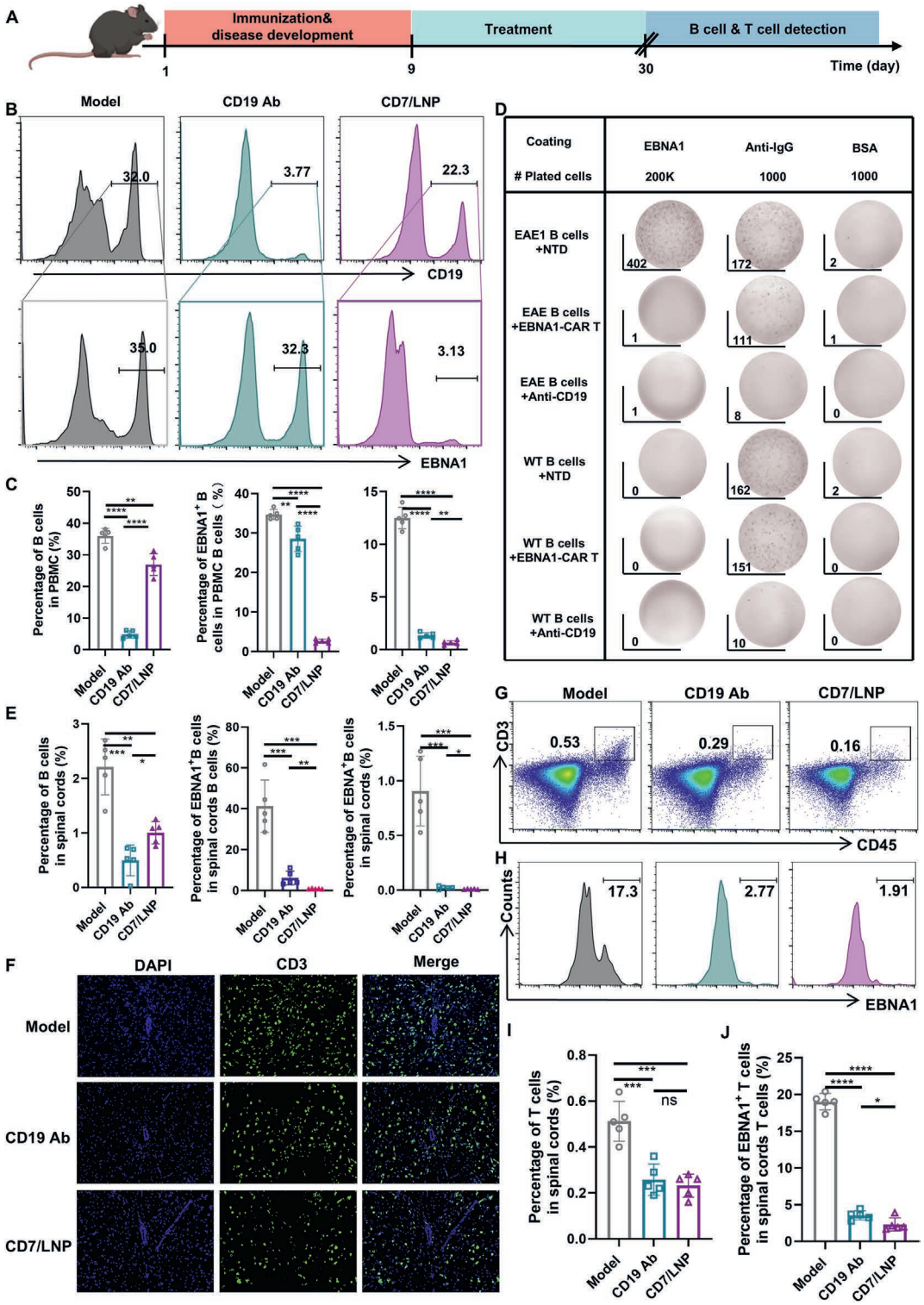

Figure 6 Deletion of anti-EBNA1-specific B cells in EAE mice. (A) Schematic representation of the procedure used to treat EAE mice and anti-EBNA1-specific B-cell detection. (B) On Day 30, peripheral blood lymphocytes of EAE mice were isolated, and the proportions of total B cells and EBNA1-specific B cells were evaluated by flow cytometry ($n = 5$ mice per group, biological replicates). (C) Quantification of total B cells and EBNA1-specific B in PBMC on Day 30 ($n = 5$ mice per group, biological replicates). Data are presented as mean ± SD, $^{**}P < 0.01$, $^{****}P < 0.0001$ *vs*. indicated. (D) B cells were further sorted with magnetic beads, and the proportions of total B cells and EBNA1-specific B cells were detected by ELISPOT assay. (E) Quantification of total B cells and EBNA1-specific B in spinal cords on Day 30 ($n = 5$ mice per group, biological replicates). Data are presented as mean ± SD, $^{*}P < 0.05$, $^{**}P < 0.01$, $^{***}P < 0.0001$ *vs*. indicated. (F) Immunofluorescence staining for T cells in spinal cord sections from EAE mice. Scale bar = 100 μm. (G–J) Spinal cords of EAE mice were harvested on Day 30 after different

treatment (Fig. 4A). Each mouse was graded every other day and assigned a clinical score ranging from 0 to 5 [28]. Treatment with CD7/LNP and CD19 Abs significantly reduced EAE scores compared with those of the PBS control (Fig. 4B). Furthermore, we demonstrate a significant decrease in maximum disease score for the CD7/LNP and CD19 Ab group compared to PBS (Fig. 4C). When comparing day of onset of maximum score, a similar significant decrease was also observed (Fig. 4D), demonstrating that treatment with CD7/LNP and CD19 Ab both dampened disease severity and disease progression.

Clinically, patients with MS present with a range of motor dysfunction symptoms[29,30]. The rotarod test was adopted to determine whether balance dysfunction was attenuated after treatment[31,32]. In the rotarod bar test, EAE mice treated with CD7/LNP and CD19 Abs spent a similar amount of time on the rotarod as WT mice spent, and most mice did not fall from the rotarod, whereas EAE mice treated with PBS fell very quickly, indicating the therapeutic efficacy of CD7/LNP in treating motor and balance dysfunction (Fig. 4E).

MS lesions are characterized by focal infiltration of monocytes and lymphocytes into sites of the brain and spinal cord[33,34]. H&E staining analysis showed fewer inflammatory foci and inflammatory immune cell infiltration in the spinal cords of CD7/LNP- and CD19 Ab-treated mice than in their counterparts (Fig. 4F and G). Demyelination is one of the key features of MS, and it ultimately leads to clinical symptoms[35]. Thus, to examine the severity of demyelination in treated mice, spinal cord sections of mice subjected to different treatments were stained for myelin using Luxol fast blue (LFB). Spinal cord sections from CD7/LNP- and CD19 Ab-treated mice exhibited a decrease in the degree of demyelination compared to that in PBS control mice (Fig. 4H). Similar results were also observed in the cerebellum (Supporting Information Fig. S23).

MS is demyelinating diseases of CNS[36]. Thus, we further observed the neuronal status after treatment by performing Nissl staining. Compared with PBS treated mice, the numbers of Nissl bodies in the spinal cords of CD7/LNP and CD19 Abs treated mice increased, and were comparable to WT mice (Fig. 4I). Moreover, CD7/LNP and CD19 Abs treatment significantly increased the expression of the two dominant central myelin proteins, proteolipid protein (PLP) and myelin basic protein (MBP), which were reduced by EAE[37,38] (Fig. 4J). These results show that CD7/LNP and CD19 Abs treatment alleviated neuronal damage and promoted a normal physiological state.

Also, the cytokine levels in the spinal cord were measured after treatment. A significant increase was observed in IFN-β levels, an EAE-resolving mediator, and a significant decrease was observed in TNF-α and IFN-γ levels, EAE-exacerbating mediators after treatment with CD7/LNP and CD19 Ab (Fig. 4K), indicating the modulation of inflammatory microenvironment in the EAE mouse model.

B-cell depletion leads to an increased risk of infection due to associated immune defects during clinical therapy. Our goal was to selectively eliminate pathogenic EBNA1$^+$ B cells *in vivo* to induce the regression of MS in EAE mouse model and to avoid the risk of infection. To evaluate the therapeutic effects, the treated mice in the CD7/LNP and CD19 Ab groups on Day 30 were chosen and injected with *Staphylococcus aureus* (SA) to evaluate their immune responses, with WT mice as the control (Fig. 5A). Among these groups, the CD7/LNP group showed comparable bactericidal activity with the WT group, whereas the activity was dramatically reduced in the CD19 Ab group (Fig. 5B and C), and higher levels of anti-bacterial related cytokines IL-4, IL-6 and TNF-α were detected in the blood of CD7/LNP and WT groups (Fig. 5D), suggesting that specific clearance of EBNA1$^+$ B cells can not only relieve symptoms but also effectively avoid the risk of infection. Moreover, the body weight and levels of the surviving mice returned to their normal, healthy state 10 days after the SA injection (Fig. 5E and F). A directly comparation of CD7/LNP-mediated CAR-T therapy with anti-CD20 therapies was conducted to further verify the efficacy, immune preservation, and safety of CAR-T therapy. As shown in Supporting Information Fig. S24, EAE mice were treated with CD7/LNP or anti-CD20 ab, both groups showed similar reductions in clinical scores, but CD7/LNP-treated mice exhibited superior resistance to Staphylococcus aureus infection.

3.5. CD7-targeted LNPs mediate EBNA1-specific B-cell elimination in EAE mice

Our goal was to selectively eliminate anti-EBNA1 B cells *in vivo* to induce the regression of MS in EAE mouse model and to avoid the risk of infection. The efficiency of anti-EBNA1 B-cell depletion was assessed at the end of treatment (Fig. 6A). We found that anti-CD19 antibodies successfully eradicated almost all circulating CD19$^+$ B cells, leaving relatively many EBNA1-positive B cells compared to the CD7/LNP group. Notably, a significant number of CD19$^+$ B cells remained after CD7/LNP treatment, while anti-EBNA1 B cells were scarce in the treated group (Fig. 6B and C).

B cells from different groups of treated mice were further evaluated for antigen-specific and total IgG B-cell depletion with ELISPOT. EBNA1 CAR-T cell treatment resulted in a 97.3% reduction in anti-EBNA1 B cells, with a 15%-20% reduction in total IgG B cells. CD19 Ab treatment depleted 95.3%−99.3% of all IgG B cells (Fig. 6D). Strikingly, an analysis of B from spinal cords the treated EAE mice showed a similar pattern of changes in total and EBNA1$^+$ cell frequencies, which may have also contributed to the amelioration of EAE (Fig. 6E, Supporting Information Figs. S25 and S26). With prior studies demonstrating EBNA1 CAR-T cytolysis of anti−EBNA1 BCR-expressing cells, as well as clinical data supporting the ability of CAR-T cells to eradicate B cells in secondary lymphoid organs and tissues, the collective data indicate that EBNA1 CAR-T effectively targets the pathogenic anti-EBNA1 B-cell population in EAE mouse model.

Self-reactive T cells that traffic to the CNS of patients with MS are driven by antigen-experienced B cells[39,40]. We profiled total cells in the spinal cord and explored whether the anti-EBNA1 B-cell depletion could interfere EBNA1 specific T cells infiltration into MS niche in EAE mouse model and further relieve EAE inflammation. As expected, CD19 Ab and CD7/LNP-treated mice showed a decrease in the number of total T cells (Fig. 6F and G, Supporting Information Fig. S27). Most notably, a decrease in the numbers of EBNA1 specific T cells were also detected in CD19

treatment ($n = 5$ mice per group, biological replicates). The cell percentages of total T cells and EBNA1 specific T cells were analyzed using FC. Data are presented as a representative plot (G, H) and as percentages (I, J). Statistical significance was analyzed using one-way ANOVA. Data are presented as mean ± SD, *$P < 0.05$, ***$P < 0.0001$, ****$P < 0.0001$ *vs.* indicated; ns, not significant.

Ab and CD7/LNP-treated mice (Fig. 6H−J), indicating that depletion of anti-EBNA1 B-cell could inhibit EBNA1 specific T cells in the MS niche in EAE mouse model, further alleviating inflammatory response.

Thus, these observations strongly support our hypothesis that selectively eliminate anti-EBNA1 B cells could induce the regression of MS and adjust the immune balance for inflammation-targeted therapy in the EAE mouse model.

4. Discussion

The success of CAR-T therapies in oncology, particularly for hematologic malignancies like B-cell leukemia and lymphoma, has revolutionized cancer treatment. However, translating this success to autoimmune diseases requires overcoming unique challenges, such as avoiding broad immunosuppression while maintaining precision. Recent studies have demonstrated the potential of CAR-T cells in autoimmune conditions, such as CD19-targeted CAR-T therapy for refractory systemic lupus erythematosus (SLE), which achieved complete remission in early trials. Our work builds on these advancements but introduces two key innovations: (I) Unlike traditional CAR-T therapies requiring *ex vivo* T-cell engineering, our CD7-targeted LNP enable *in situ* generation of CAR-T cells, eliminating the need for leukapheresis and reducing manufacturing complexity. (II) By targeting EBNA1$^+$ B cells-a pathogenic subset implicated in MS—we avoid the pan-B-cell depletion caused by anti-CD20 therapies, thereby preserving protective immune functions.

The physiological functions of B cells and the main mechanisms through which B cells are thought to contribute to CNS autoimmunity have been gradually investigated. The proinflammatory functions of B cells, including the presentation of critical antigens to Th17 and Th1 cells, secretion of cytokines and other molecules, and antibody production, are mediators of tissue damage in many neurologic disorders[40-42]. However, experimental and clinical efforts used thus far to clear activated B cells, such as radiation and CD20 mAbs have the potential to increase the risk of off-target effects on the immune system, resulting in immune deficiency[42-45].

Ongoing researches from different fields have provided compelling evidence that EBV, a herpesvirus that infects more than 90% of the global population, is a leading cause of MS[4,46,47]. Over the past few years, a number of studies have provided clues on the underlying mechanisms, and understanding EBV-specific immune control could provide insights into the mechanisms that underlie the increased risk of MS owing to EBV infection, which might help us to develop more targeted treatments for MS. Two new studies reinvigorated this interest and provide robust epidemiological evidence and a mechanistic link that that antibodies derived from the cerebrospinal fluid of patients with MS can recognize both the EBV nuclear antigen 1 (EBNA1) as well as the host CNS cellular protein GlialCAM with high affinity[3,4]. Judith A. James's lab found anti-EBNA1 responses are related to myelin basic protein autoantibodies in MS patients and EBNA1$_{411-426}$ immunization causes clinical signs of MS like disease in mice[48]. EBNA1-specific B cells express an anti-EBNA1 B cell receptor (BCR), a membrane-bound autoantibody, which suggests that EBNA1 antibody-producing B cells are immune cells for MS and may be a potential implication for MS therapy. Given the evidence that EBV plays a central role in triggering MS, we report a novel precision cellular immunotherapy for autoantigen-specific B cell depletion in EBNA1 involved MS in EAE mouse model, which was achieved by engineering EBNA1 CAR-T cells *in vivo* by using targeted LNPs.

We found nanoparticle-transfected T cells were fully functional, as they selectively killed EBNA1 specific cells from EAE mice at levels similar to T cells transduced with a lentiviral vector encoding the same CAR (Fig. S15). When the targeted LNPs were injected *in vivo* once, CAR expression on circulating T cells was dynamically detected and verified during 10 days of detection and thus it is superior to other treatments that need repeated administrations. Further, we found a substantial number of peripheral CD19$^+$ B cells remained without anti-EBNA1 B cells after targeted LNPs treated in EAE mice (Fig. 6B−D), which had compared ability of anti-infection with WT mice. These experimental results provide a proof of concept that circRNA encapsulated in designated LNPs can be conveyed intravenously to produce functional engineered lymphocytes *in vivo*. By focusing on LNPs to explicit cell types, as we show here for T lymphocytes, altered mRNA therapeutics are probably going to have extensive applications. The generation of engineered lymphocytes, as we reported T cells, *in vivo* using RNA is attractive for limiting toxicities, including risks incurred by lymphodepletion before injection, and allow for precise dosing. Dissimilar to patients with malignant growth, those suffering from autoimmune diseases do not require a total disposal of lymphocytes. Besides, targeted LNP/RNA technology affords the advantageous ability to titrate dosing and to re-dose as needed[49,50]. Future investigations will be expected to optimize the dosing strategy, composition of LNP, and targeting approaches to further enhance therapeutic effects and limit potential toxicities.

Our study has limitations. Auto-immune B cells may contribute to pathogenesis via antigen presentation and production of proinflammatory cytokines. In this study, we demonstrate EBNA1 specific B cells are critical drivers of our EBNA1 induced MS mouse models. However, these B cell effector functions are not featured well in EBNA1 induced EAE development. Peters's group developed an adoptive cotransfer system which described overexpression of the proinflammatory cytokine IL-6 by autoreactive B cells leads to an accelerated EAE but does not affect the T cell response[51]. Kuchroo's group demonstrated the active cooperation between antigen-specific T and B cells induce a distinct clinicopathologic EAE pattern in their reported EAE model[52]. Whether these EBNA1 specific B cells in our EAE mice accelerate EAE by cooperating with T cells that closely replicates human or by secreting proinflammatory cytokines need to be further studied.

5. Conclusions

In this study, we tested the possible use of EBNA1 CAR-T cells to treat MS in an EAE mouse model. Our approach achieved (I) EBNA1 CAR-T-cell programming *in situ* with low off-target effects, (II) specific EBNA1 specific B-cell depletion *in vivo*, and (III) reduced disease symptoms without the risk of infection, representing a "off-the-shelf" universal therapeutic capable platform technology and warrant further clinical trials.

Acknowledgments

This work was supported by the National Natural Science Foundation of China (82504679, 82425056, 82350125, 82173763, 82372020), the Shenzhen Medical Research Fund (A2503048), the Shenzhen Science and Technology Program

(JCYJ20250604183451068), the Fundamental Research Funds of Shandong Province (ZR2022ZD18), the China Postdoctoral Science Foundation (2025M783556, 2023M732091), and the China National Postdoctoral Program for Innovative Talents (BX20230204), Taishan Scholar Young Expert (tsqn202408343). We appreciate the technical support from Xu Mei, Yang Yu, Jin Zhang, Meng Li, Lin Wang and Lin Wu in Advanced Medical Research Institute/Translational Medicine Core Facility of Advanced Medical Research Institute, Shandong University. We are also grateful for technical support from X. Wang and F. Cui from the Pharmaceutical Biology Sharing Platform, School of Pharmaceutical Sciences, Shandong University.

Author contributions

Xinyi Jiang, Anning Li and Chongdeng Shi conceived the project and designed the experiments. Chen Chen, Chongdeng Shi, Hui Yang, Maosen Han, Anning Li, Xiaotian Zhao, Zuolin Zheng, Kun Zhao, Fei Yang and Yudong Song performed the experiments. Chen Chen, Chongdeng Shi, Huijun Wang, Zhipeng Fu, Kuan Dai, Fei Yang, Na Li and Xinyi Jiang analyzed and interpreted the data in this study. Anning Li, Chongdeng Shi, Fei Yang, Yudong Song and Xinyi Jiang wrote the manuscript draft. The final draft of the manuscript was approved by all coauthors.

Conflicts of interest

The authors declare no competing interests.

Appendix A. Supporting information

Supporting information to this article can be found online at https://doi.org/10.1016/j.apsb.2026.03.033.

References

1. Rodríguez Murúa S, Farez MF, Quintana FJ. The immune response in multiple sclerosis. *Annu Rev Pathol* 2022;**17**:121−39.
2. The Lancet N. Multiple sclerosis under the spotlight. *Lancet Neurol* 2021;**20**:497.
3. Lanz TV, Brewer RC, Ho PP, Moon JS, Jude KM, Fernandez D, et al. Clonally expanded B cells in multiple sclerosis bind EBV EBNA1 and GlialCAM. *Nature* 2022;**603**:321−7.
4. Bjornevik K, Cortese M, Healy BC, Kuhle J, Mina MJ, Leng Y, et al. Longitudinal analysis reveals high prevalence of Epstein−Barr virus associated with multiple sclerosis. *Science* 2022;**375**:296−301.
5. Wekerle H. Epstein−Barr virus sparks brain autoimmunity in multiple sclerosis. *Nature* 2022;**603**:230−2.
6. Kuchroo VK, Weiner HL. How does Epstein−Barr virus trigger MS?. *Immunity* 2022;**55**:390−2.
7. Gelfand JM, Cree BAC, Hauser SL. Ocrelizumab and other $CD20^+$ B-cell-depleting therapies in multiple sclerosis. *Neurotherapeutics* 2017;**14**:835−41.
8. Chisari CG, Sgarlata E, Arena S, Toscano S, Luca M, Patti F. Rituximab for the treatment of multiple sclerosis: a review. *J Neurol* 2022;**269**:159−83.
9. Margoni M, Preziosa P, Filippi M, Rocca MA. Anti-CD20 therapies for multiple sclerosis: current status and future perspectives. *J Neurol* 2022;**269**:1316−34.
10. Lamb YN. Ocrelizumab: a review in multiple sclerosis. *Drugs* 2022; **82**:323−34.
11. Leffler J, Trend S, Hart PH, French MA. Epstein−Barr virus infection, B-cell dysfunction and other risk factors converge in gut-associated lymphoid tissue to drive the immunopathogenesis of multiple sclerosis: a hypothesis. *Clin Transl Immunol* 2022;**11**:e1418.
12. Exley AR, Rantell K, McBlane J. Clinical development of cell therapies for cancer: the regulators' perspective. *Eur J Cancer* 2020;**138**: 41−53.
13. Khang M, Suryaprakash S, Kotrappa M, Mulyasasmita W, Topp S, Wu J. Manufacturing innovation to drive down cell therapy costs. *Trends Biotechnol* 2023;**41**:1216−9.
14. Zhao Z, Chen Y, Francisco NM, Zhang Y, Wu M. The application of CAR-T cell therapy in hematological malignancies: advantages and challenges. *Acta Pharm Sin B* 2018;**8**:539−51.
15. Short L, Holt RA, Cullis PR, Evgin L. Direct *in vivo* CAR T cell engineering. *Trends Pharmacol Sci* 2024;**45**:406−18.
16. Billingsley MM, Singh N, Ravikumar P, Zhang R, June CH, Mitchell MJ. Ionizable lipid nanoparticle-mediated mRNA delivery for human CAR T cell engineering. *Nano Lett* 2020;**20**:1578−89.
17. Suzuki H, Zelphati O, Hildebrand G, Leserman L. CD4 and CD7 molecules as targets for drug delivery from antibody bearing liposomes. *Exp Cell Res* 1991;**193**:112−9.
18. Preijers FW, Tax WJ, De Witte T, Janssen A, vd Heijden H, Vidal H, et al. Relationship between internalization and cytotoxicity of ricin A-chain immunotoxins. *Br J Haematol* 1988;**70**:289−94.
19. Mayer KE, Mall S, Yusufi N, Gosmann D, Steiger K, Russelli L, et al. T-cell functionality testing is highly relevant to developing novel immunotracers monitoring T cells in the context of immunotherapies and revealed CD7 as an attractive target. *Theranostics* 2018;**8**:6070−87.
20. Eugster HP, Frei K, Kopf M, Lassmann H, Fontana A. IL-6-deficient mice resist myelin oligodendrocyte glycoprotein-induced autoimmune encephalomyelitis. *Eur J Immunol* 1998;**28**:2178−87.
21. Langenfurth A, Rinnenthal JL, Vinnakota K, Prinz V, Carlo AS, Stadelmann C, et al. Membrane-type 1 metalloproteinase is upregulated in microglia/brain macrophages in neurodegenerative and neuroinflammatory diseases. *J Neurosci Res* 2014;**92**:275−86.
22. Rurik JG, Tombácz I, Yadegari A, Méndez Fernández PO, Shewale SV, Li L, et al. CAR T cells produced *in vivo* to treat cardiac injury. *Science* 2022;**375**:91−6.
23. Liu J, Zhang Y, Liu C, Jiang Y, Wang Z, Guo Z, et al. A single dose of VEGF-A circular RNA sustains *in situ* long-term expression of protein to accelerate diabetic wound healing. *J Control Release* 2024;**373**: 319−35.
24. Sapozhnikov DM, Szyf M. Enzyme-free targeted DNA demethylation using CRISPR−dCas9-based steric hindrance to identify DNA methylation marks causal to altered gene expression. *Nat Protoc* 2022; **17**:2840−81.
25. Zuo Z, Yin H, Zhang Y, Xie C, Wang Q. A cytotoxic T cell inspired oncolytic nanosystem promotes lytic cell death by lipid peroxidation and elicits antitumor immune responses. *Nat Commun* 2023;**14**:5456.
26. VanPortfliet JJ, Lei Y, Ramanathan M, Martinez CG, Wong J, Stodola TJ, et al. Caspase-11 drives macrophage hyperinflammation in models of Polg-related mitochondrial disease. *Nat Commun* 2025;**16**: 4640.
27. Smith TT, Stephan SB, Moffett HF, McKnight LE, Ji W, Reiman D, et al. *In situ* programming of leukaemia-specific T cells using synthetic DNA nanocarriers. *Nat Nanotechnol* 2017;**12**:813−20.
28. Clarkson BD, Grund EM, Standiford MM, Mirchia K, Westphal MS, Muschler ES, et al. $CD8^+$ T cells recognizing a neuron-restricted antigen injure axons in a model of multiple sclerosis. *J Clin Investig* 2023;**21**:e162788.
29. Marchesi O, Bonacchi R, Valsasina P, Rocca MA, Filippi M. Resting state effective connectivity abnormalities of the Papez circuit and cognitive performance in multiple sclerosis. *Mol Psychiatr* 2022;**27**: 3913−9.
30. Solomon AJ, Arrambide G, Brownlee WJ, Flanagan EP, Amato MP, Amezcua L, et al. Differential diagnosis of suspected multiple sclerosis: an updated consensus approach. *Lancet Neurol* 2023;**22**: 750−68.
31. Hsu SJ, Zhang C, Jeong J, Lee SI, McConnell M, Utsumi T, et al. Enhanced meningeal lymphatic drainage ameliorates

neuroinflammation and hepatic encephalopathy in cirrhotic rats. *Gastroenterology* 2021;**160**:1315−29.e13.
32. Guo W, Hu C, Wang Y, Zhang W, Zhang S, Peng J, et al. NO-releasing double-crosslinked responsive hydrogels accelerate the treatment and repair of ischemic stroke. *Acta Pharm Sin B* 2025;**15**:1112−25.
33. Prinz M, Priller J. The role of peripheral immune cells in the CNS in steady state and disease. *Nat Neurosci* 2017;**20**:136−44.
34. Ramaglia V, Rojas O, Naouar I, Gommerman JL. The ins and outs of central nervous system inflammation-lessons learned from multiple sclerosis. *Annu Rev Immunol* 2021;**39**:199−226.
35. Attfield KE, Jensen LT, Kaufmann M, Friese MA, Fugger L. The immunology of multiple sclerosis. *Nat Rev Immunol* 2022;**22**:734−50.
36. Lünemann JD, Ruck T, Muraro PA, Bar-Or A, Wiendl H. Immune reconstitution therapies: concepts for durable remission in multiple sclerosis. *Nat Rev Immunol* 2020;**16**:56−62.
37. Kuhlmann T, Ludwin S, Prat A, Antel J, Brück W, Lassmann H. An updated histological classification system for multiple sclerosis lesions. *Acta Neuropathol* 2017;**133**:13−24.
38. Kilsdonk ID, Jonkman LE, Klaver R, van Veluw SJ, Zwanenburg JJ, Kuijer JP, et al. Increased cortical grey matter lesion detection in multiple sclerosis with 7 T MRI: a post-mortem verification study. *Brain* 2016;**139**:1472−81.
39. Pappalardo JL, O'Connor KC. B cells drive auto-T cells to the brain. *Sci Immunol* 2018;**3**:eaav4512.
40. Jelcic I, Al Nimer F, Wang J, Lentsch V, Planas R, Jelcic I, et al. Memory B cells activate brain-homing, autoreactive $CD4^+$ T cells in multiple sclerosis. *Cell* 2018;**175**:85−100.e23.
41. Mauri C, Bosma A. Immune regulatory function of B cells. *Annu Rev Immunol* 2012;**30**:221−41.
42. Bhargava P, Hartung HP, Calabresi PA. Contribution of B cells to cortical damage in multiple sclerosis. *Brain* 2022;**145**:3363−73.
43. Li R, Rezk A, Miyazaki Y, Hilgenberg E, Touil H, Shen P, et al. Proinflammatory GM-CSF-producing B cells in multiple sclerosis and B cell depletion therapy. *Sci Transl Med* 2015;**7**:310ra166.
44. Lin M, Zhang J, Zhang Y, Luo J, Shi S. Ocrelizumab for multiple sclerosis. *Cochrane Database Syst Rev* 2022;**5**:Cd013247.
45. Hauser SL, Cree BAC. Treatment of multiple sclerosis: a review. *Am J Med* 2020;**133**:1380−90.e2.
46. Soldan SS, Lieberman PM. Epstein−Barr virus and multiple sclerosis. *Nat Rev Microbiol* 2023;**21**:51−64.
47. Sollid LM. Epstein−Barr virus as a driver of multiple sclerosis. *Sci Immunol* 2022;**7**:eabo7799.
48. Jog NR, McClain MT, Heinlen LD, Gross T, Towner R, Guthridge JM, et al. Epstein Barr virus nuclear antigen 1 (EBNA-1) peptides recognized by adult multiple sclerosis patient sera induce neurologic symptoms in a murine model. *J Autoimmun* 2020;**106**:102332.
49. Xiao Y, Wu B, Zhou Q, Wu F, Li N, Xu C, et al. Technologies for chimeric antigen receptor transgene delivery. *Trends Mol Med* 2025;**31**:1047−64.
50. Xu S, Hu Z, Song F, Xu Y, Han X. Lipid nanoparticles: composition, formulation, and application. *Mol Ther, Methods Clin Dev* 2025;**33**:101463.
51. Thomann AS, McQuade CA, Pinjušić K, Kolz A, Schmitz R, Kitamura D, et al. A B cell-driven EAE mouse model reveals the impact of B cell-derived cytokines on CNS autoimmunity. *Proc Natl Acad Sci USA* 2023;**120**:e2300733120.
52. Bettelli E, Baeten D, Jäger A, Sobel RA, Kuchroo VK. Myelin oligodendrocyte glycoprotein-specific T and B cells cooperate to induce a Devic-like disease in mice. *J Clin Investig* 2006;**116**:2393−402.